Stromal Fibroblasts Mediate Anti–PD-1 Resistance via MMP-9 and Dictate TGFβ Inhibitor Sequencing in Melanoma

Fei Zhao[1], Kathy Evans[1], Christine Xiao[1], Nicholas DeVito[1], Balamayooran Theivanthiran[1], Alisha Holtzhausen[2], Peter J. Siska[3], Gerard C. Blobe[1,4], and Brent A. Hanks[1,4]

Abstract

Although anti–PD-1 therapy has improved clinical outcomes for select patients with advanced cancer, many patients exhibit either primary or adaptive resistance to checkpoint inhibitor immunotherapy. The role of the tumor stroma in the development of these mechanisms of resistance to checkpoint inhibitors remains unclear. We demonstrated that pharmacologic inhibition of the TGFβ signaling pathway synergistically enhanced the efficacy of anti–CTLA-4 immunotherapy but failed to augment anti–PD-1/PD-L1 responses in an autochthonous model of BRAF^V600E melanoma. Additional mechanistic studies revealed that TGFβ pathway inhibition promoted the proliferative expansion of stromal fibroblasts, thereby facilitating MMP-9–dependent cleavage of PD-L1 surface expression, leading to anti–PD-1 resistance in this model. Further work demonstrated that melanomas escaping anti–PD-1 therapy exhibited a mesenchymal phenotype associated with enhanced TGFβ signaling activity. Delayed TGFβ inhibitor therapy, following anti–PD-1 escape, better served to control further disease progression and was superior to a continuous combination of anti–PD-1 and TGFβ inhibition. This work illustrates that formulating immunotherapy combination regimens to enhance the efficacy of checkpoint blockade requires an in-depth understanding of the impact of these agents on the tumor microenvironment. These data indicated that stromal fibroblast MMP-9 may desensitize tumors to anti–PD-1 and suggests that TGFβ inhibition may generate greater immunologic efficacy when administered following the development of acquired anti–PD-1 resistance. *Cancer Immunol Res; 6(12); 1459–71. ©2018 AACR.*

See related Spotlight on p. 1444

Introduction

The introduction of the anti–CTLA-4 and anti–PD-1 checkpoint inhibitors has significantly improved the overall survival of patients with advanced melanoma (1, 2). Despite these additions to our treatment armamentarium, most advanced cancer patients remain resistant to checkpoint inhibitor therapies (3). Many aspects of the fundamental mechanisms involved in primary and secondary resistance to these immunotherapies remain poorly understood (4, 5). Studies are currently attempting to identify strategies that synergize with the available checkpoint inhibitors. However, determining which biological pathways to manipulate is challenging, and no clear approach to designing combinatorial immunotherapy regimens currently exist (6, 7). An improved understanding of the tumor-mediated mechanisms of immuno-

therapy resistance will ultimately provide a guide for selecting a rational regimen for a specific patient.

Our previous work, as well as the work of others, has implicated transforming growth factor-β (TGFβ) as playing an important role in the generation of an immunotolerant tumor microenvironment (TME) that facilitates disease progression (8–10). TGFβ effectively suppresses the activity of several components of the host immune system, including CD8+ T cells, while driving the differentiation of immunosuppressive CD4+FoxP3+ regulatory T cells (11). Based on these data, we hypothesized that inhibiting TGFβ signaling would be a promising strategy for augmenting the efficacy of checkpoint inhibition (12). Several approaches have been investigated for inhibiting TGFβ signaling, including the development of large-molecule TGFβ inhibitors, such as the human TGFβ antibody GC1008 (fresolimumab), as well as the selective small-molecule type I TGFβ serine/threonine kinase inhibitors TEW-7197 (vactosertib) and LY2157299 monohydrate (galunisertib; refs. 13–15).

Tumor-associated fibroblasts (TAF) have been previously implicated in establishing an immunosuppressive TME (16, 17). Studies have shown that TAFs contribute to the development of a physical barrier that interferes with immune cell infiltration, directly inhibiting T-cell trafficking, and expressing an array of factors, including CCL2, that contribute to the establishment of an immunotolerant state (18). Studies have also demonstrated that activated fibroblasts associated with an autochthonous model of pancreatic ductal adenocarcinoma promote CD8+ T-cell exclusion, based on a mechanism that depends upon CXCL12 chemokine expression (19). This work further showed that FAP+ fibroblasts eliminate responses to anti–PD-1

[1]Department of Medicine, Division of Medical Oncology, Duke Cancer Institute, Duke University Medical Center, Durham, North Carolina. [2]Lineberger Comprehensive Cancer Center, University of North Carolina at Chapel Hill, Chapel Hill, North Carolina. [3]Department of Internal Medicine III, University Hospital Regensburg, Regensburg, Germany. [4]Department of Pharmacology and Cancer Biology, Duke University, Durham, North Carolina.

Corresponding Author: Brent A. Hanks, Duke University Medical Center, 308 Research Drive, LSRC, Room C203, Box 91004, Durham, NC 27708. Phone: 919-684-1995; Fax: 919-613-1728; E-mail: hanks004@mc.duke.edu

and anti–CTLA-4 in this tumor model (20). Melanoma-associated fibroblasts (MAF) have also been demonstrated to play an important role in the induction of immune suppression via melanoma–stroma cross-talk and RNA-seq studies have related TAF abundance with targeted drug resistance, as well as checkpoint inhibitor resistance in advanced melanoma (21, 22). Despite this insight into the immunosuppressive properties of stromal fibroblasts, the mechanisms that TAFs utilize to suppress checkpoint inhibitor responses remain unclear, and whether TAFs play a role in adaptive resistance to checkpoint inhibitor therapies has not been investigated. In the current study, we explored the impact of small-molecule inhibition of TGFβ signaling on the local TME, and how the alterations involving TAFs contributed to the efficacy of checkpoint inhibition in an autochthonous model of BRAF^{V600E} melanoma.

Materials and Methods

Reagents

TEW-7197 (EW-7197), a serine/threonine type I TGFβ receptor inhibitor, was provided by MedPacto Inc. LY2157299 monohydrate, also a serine/threonine type I TGFβ receptor inhibitor, was provided by Eli Lilly and Company. An MMP-9 inhibitor (cat. #sc-311437) was purchased from Santa Cruz Biotechnology and titrated in coculture assays between 0 and 50 nmol/L, and the MMP-13 inhibitor (cat. #444283) was purchased from Sigma-Aldrich and titrated in coculture assays between 0 and 80 μmol/L.

Mice

All mice were housed in a specific pathogen-free facility at Duke University. BALB/cJ (H-2^d), C57BL/6J (C57, H-2^b), and *Braf^{tm1Mmcm} Pten^{tm1Hwu}*Tg(Tyr-cre/ERT2)13Bos/BosJ (RRID: IMSR_JAX:013590, *Braf^{V600E}Pten$^{-/-}$*, H-2^b) mice were purchased from The Jackson Laboratory. Littermates, 6 to 8 weeks old, from both sexes were randomly chosen for all experiments and were performed based on a protocol approved by the Institutional Animal Care and Use Committee at Duke University.

Cell lines

Braf^{V600E}Pten$^{-/-}$ (BPD6, male) cell lines were generated and cultured in RPMI with 10% FBS as previously described (23). Melanoma-associated fibroblasts (*Braf^{V600E}Pten$^{-/-}$*/MAFs) were generated from *Braf^{tm1Mmcm} Pten^{tm1Hwu}* Tg(Tyr-cre/ERT2)13Bos/BosJ mice. Central tissue from a primary melanoma lesion was resected, diced into 1-mm^3 pieces, and rinsed with DMEM (1× antibiotic–antimycotic, 10% FBS). The tissue was cultured in a 100-mm cell culture dish for 5 days, remaining melanoma tissue was removed, and attached cells were expanded. After five passages, cells were trypsinized and enriched by CD90.2 microbeads (STEMCELL Technologies, cat. #18951) according to the manufacture's protocol. CD45$^-$EpCAM$^-$CD90.2$^+$ cell purity was greater than 90% by flow cytometry. The *Braf^{V600E}Pten$^{-/-}$*/MAF cell line was found to exhibit the expected spindle morphology by light microscopy and screened positive for elevated expression levels of α-SMA and vimentin by Western blot. Genetic silencing of *Mmp9* expression by *Braf^{V600E}Pten$^{-/-}$*/MAF cells was performed using an *Mmp9*-targeted shRNA-expressing lentiviral vector (Sigma-Aldrich) followed by puromycin selection to generate the *Braf^{V600E}Pten$^{-/-}$*/MAF^{MMP9KD} cell line. All cell lines used in this study were tested *Mycoplasma*-free annually by Duke University Cell Culture Facility shared services. All cell lines were cultured less than 2 weeks before experimental execution.

Syngeneic transplant tumor models

Braf^{V600E}Pten$^{-/-}$ cells (5×10^5 cells) were implanted by subcutaneous (s.c.) injection at the base of the tail of syngeneic C57BL/6 mice. For cotransplant studies, 5×10^5 *Braf^{V600E}Pten$^{-/-}$* cells and 1.5×10^6 *Braf^{V600E}Pten$^{-/-}$*/MAF melanoma fibroblasts were premixed in Matrigel (Corning) and delivered by s.c. injection into C57BL/6 mice. Tumor growth was monitored by caliper measurement every 3 days, and treatment was initiated when tumor volumes reached 64 mm^3. Tumor volume was calculated according to the formula: cm^3 = [(length (cm) × (width (cm))^2]/2. TEW-7197 was administered daily by oral gavage (25 mg/kg/day). Rat anti–PD-1 (Bio X Cell, clone RMP-14) or rat IgG2a isotype control (Bio X Cell) was delivered every 3 days by intraperitoneal (i.p.) injection (250 μg/dose). Hamster anti–CTLA-4 (Bio X Cell, clone 9H10) or hamster IgG1 isotype control (Bio X Cell) was also delivered every 3 days by i.p. injection (100 μg/dose). Experiments were terminated between 28 and 33 days after implantation.

Autochthonous tumor model

B6.Cg-*Braf^{tm1Mmcm} Pten^{tm1Hwu}* Tg(Tyr-cre/ERT2 H-2^b)13Bos/BosJ (*Braf^{V600E}Pten$^{-/-}$*, H-2^b), transgenic mice were subdermally injected with 4-HT (38.75 μg/mouse; Sigma-Aldrich) to induce primary melanoma development at the base of the tail. Melanoma growth was monitored by orthogonal caliper measurements every 3 days between days 15 and 32. All mice were treated as described above. Tumor escape from anti–PD-1 therapy was found to occur by day 21. Delayed TEW-7197 therapy was initiated on day 23. Experiments were terminated between 28 and 33 days.

Murine cell isolation

Tumors were resected and mechanically disaggregated by a gentleMACS dissociator (Miltenyi), filtered through 70-μm filters, and digested with RPMI containing collagenase IV (1 mg/mL, Sigma-Aldrich), hyaluronidase (0.1 mg/mL, Sigma-Aldrich), and deoxyribonuclease (20 U/mL, Sigma-Aldrich) on a shaker at 250 rpm at 37°C for 1 hour (23). Resected splenic and lymph node tissues were mechanically disaggregated using 1 cc syringe plunger and 40-μm filters followed by treatment with RBC lysis buffer (Sigma-Aldrich).

Antibodies and immunoblot analysis

Primary antibodies included TGFβ (Cell Signaling Technology, cat. #3711), total SMAD2 (Cell Signaling Technology, cat. #5339), phospho-SMAD2 (S465/467; Cell Signaling Technology, cat. #3108), β-actin (Millipore, cat. #MABT1333), and MMP-9 (Millipore, cat. #MABT171) and were used at 1:1,000. Secondary antibodies included goat anti-rabbit IgG-HRP (Bio-Rad, cat. #172-1019) and goat anti-mouse IgG-HRP (Bio-Rad, cat. #170-6516) and were used at 1:5,000. Cells were lysed in Laemmli sample buffer (250 mmol/L Tris–HCl, pH 6.8, 10% SDS, 30% (v/v) glycerol, 10 mmol/L DTT, 0.05% (w/v) bromophenol blue) after treatment and subjected to SDS-polyacrylamide gel electrophoresis and immunoblot analysis. Immunoblots were visualized by chemiluminescence substrate (Thermo Fisher) and imaged by a ChemiDoc XRSplus system (Bio-Rad).

Transwell migration and coculture assays

The $Braf^{V600E}Pten^{-/-}$ cell line was incubated with increasing concentrations of TEW-7197 for 24 hours, briefly rinsed, and coincubated for 18 hours at 37°C with the $Braf^{V600E}Pten^{-/-}$/MAF cell line seeded onto an 8-μm transwell insert. Transwell insert membranes were removed, and the outer membrane was stained with Wright–Giemsa and fixed with methanol. Membranes were mounted to slides, and cells were quantitated at 40× magnification. For PD-L1 flow cytometry studies, $Braf^{V600E}Pten^{-/-}$ cells were stained with CellTracker Violet (Thermo Fisher) according to the manufacturer's protocol and incubated with $Braf^{V600E}Pten^{-/-}$/MAF cells at a 1:3 ratio at 37°C in DMEM media with 10% FBS for 48 hours before collection and analysis. For $Mmp9$ qRT-PCR studies, $Braf^{V600E}Pten^{-/-}$ cells were cocultured with $Braf^{V600E}Pten^{-/-}$/MAF cells in a 0.4-μm transwell insert at a ratio of 1:3 at 37°C in DMEM media with 10% FBS for 48 hours before $Braf^{V600E}Pten^{-/-}$ cells were collected.

Flow cytometry

All antibodies used for flow cytometry were purchased from BD Pharmingen and included CD3–PerCP-Cy5.5 (cat. #561108), CD4-FITC (cat. #553047), CD8-APC (cat. #553035), CD8-BV510 (cat. #563068), CD45–APC-Cy7 (cat. #557659), CD45-PE (cat. #553081), CD90.2-FITC (cat. #553003), CD326 (EpCAM)-APC (cat. #563478), FoxP3-PE (cat. #560408), and PD-L1–PE (cat. #558091). One million cells were stained with 1 μg of each fluorochrome-conjugated antibody and analyzed using a FACSCanto II (Becton Dickinson). Cell-surface staining was performed by incubating tumor-derived cell populations with selected antibodies on ice in the dark for 30 minutes in PBS and 0.5% FBS (HyClone GE Healthcare Life Sciences). Intracellular staining of FoxP3 was performed using a mouse FoxP3 fixation and permeabilization kit (BD Pharmingen, cat. #560409). Nonviable cells were excluded from further flow analysis using a Live/Dead Fixable Violet Dead Cell Stain Kit (Thermo Fisher; cat. #L34955). Data were analyzed using FlowJo version 10.1r7 (FlowJo, LLC).

Immunohistochemistry(IHC)/immunofluorescence (IF)

Paraffin-embedded tissues were processed and stained following standard protocols and imaged with a Zeiss CLSM 700 confocal microscope. The following antibodies were used in IHC and immunofluorescence experiments: TGFβ (Abcam; cat. #ab66043; 2 μg/mL), CD8a (BioLegend; cat. #100702; 1:50), PD-L1 (Abcam; cat. #ab80276; 1:50), vimentin (Cell Signaling; cat. #5741; 1:100), and αSMA (Novus Biologicals; cat. #NB600-1434; 1:200). The PD-L1 IHC score was quantified in a blinded fashion based on an evaluation of both the frequency of cells expressing PD-L1 on a 0 to 5 scale and the intensity of PD-L1 staining on a 1 to 3 scale (24).

RNA isolation and qRT-PCR

Total RNA was isolated by the RNeasy Plus Mini Kit (Qiagen) for qRT-PCR and RNA-seq. RNA (500 ng) was used in cDNA synthesis reactions (iScript, Bio-Rad). Real-time PCR was performed using an ABI7500 Real-Time PCR system (Life Technologies; Supplementary Table S1). All data were normalized to $Actb$ expression, and relative gene expression was quantitated based on the $2^{-\Delta\Delta Ct}$ method.

RNA-seq assays

RNA-seq was performed by Duke Sequencing and Genomic Technologies Shared Resources. A complementary DNA library was prepared via oligo-dT–directed reverse transcription (Ambion) and subjected to deep sequencing on Illumina HiSeq4000 (50-bp single-read sequencing; Anti–PD-1 resistance Study RNA-seq, accession number: SAMN09878780; Melanoma Fibroblast Co-Transplant Tumor Study RNA-seq, accession number: SAMN09879305). RNA-seq data generated here and publicly available RNA-seq data (22) were processed by Duke Center for Genomic and Computational Biology using the TrimGalore toolkit that uses Cutadapt to trim low-quality bases and Illumina sequencing adapters from the 3′ end of the reads. Only reads that were 20 nucleotides (nt) or longer after trimming were kept for further analysis. Reads were mapped to the GRCm38v68 version of the mouse genome and transcriptome using the STAR RNA-seq alignment tool. Reads were kept for subsequent analysis if they mapped to a single genomic location. Gene counts were compiled using the HTSeq tool. Only genes that had at least 10 reads in any given library were used in subsequent analysis. Normalization and differential expression was carried out using the DESeq2 Bioconductor package with the R statistical programming environment. The false discovery rate was calculated to control for multiple hypothesis testing. Gene set enrichment analysis was performed to identify differentially regulated pathways and gene ontology terms for each of the comparisons performed (25).

In vivo proliferation assays

Proliferation rate of TAF was measured by the EdU-Click kit (Baseclick). Tumor-bearing $Braf^{V600E}Pten^{-/-}$ mice were treated with EdU 50 mg/kg/dose by i.p. injection 96 and 24 hours before harvest. Single-cell suspensions were generated as previously described, fixed, permeabilized, and subjected to EdU detection according to the manufacturer's protocol.

ELISPOT assays

A mouse IFNγ ELISPOT^{PLUS} (MABTECH) was performed according to the manufacturer's guidelines. In brief, single-cell suspensions of splenocytes, generated by mechanical dissociation followed by RBC lysis using ammonium chloride, were plated at 250,000 cells/well on an ELISPOT plate (MABTECH) and incubated for 24 hours at 37°C with the following peptides: TRP2$_{180-188}$ peptide (1 μg/mL, SVYDFFVWL; ANASPEC), ConA-positive control, or the irrelevant negative control OVA$_{257-264}$ peptide (1 μg/mL, SIINFEKL, InvivoGen). Imaging was conducted using a CTL ImmunoSpot S5 core (ImmunoSpot) and quantified using ImmunoCapture and ImmunoSpot software (ImmunoSpot).

Statistical analysis

GraphPad Prism 7 Windows version was used for all statistical analyses. Unpaired t tests were used to compare mean differences between control and treatment groups. Univariate ANOVA followed by Tukey post hoc test was performed to analyze data containing three or more groups. Spearman correlation analysis was used to correlate levels of TGFβ expression with tumor volume. Differences in overall survival were displayed using a Kaplan–Meier plot and calculated based on a log-rank test. The significance threshold for all statistical calculations was based on a P value of 0.05, and all tests were two-sided.

Zhao et al.

Results

TGFβ inhibition synergistically enhances anti–CTLA-4 immunotherapy

We found that anti–CTLA-4 monotherapy failed to control disease progression in the autochthonous $Braf^{V600E}Pten^{-/-}$ melanoma model (Fig. 1A). IHC and whole-tissue Western blots demonstrated that these melanoma tissues expressed TGFβ (Fig. 1B). Given our previous data implicating an important role for TGFβ in the establishment of an immunotolerant TME, we sought to determine the impact of TGFβ inhibition in the same melanoma model (26). Despite the ability of the TEW-7197 type I TGFβ receptor (TBRI) serine/threonine kinase inhibitor to effectively block downstream TGFβ signaling within developing melanoma tissues based on SMAD2 phosphorylation (Fig. 1C), this agent exhibited no impact on primary melanoma growth when given alone (Fig. 1D). However, when the TBRI inhibitor was administered in combination with anti–CTLA-4, we observed a suppression of primary melanoma growth, a reduction of pulmonary metastatic lesions, and a significant improvement in the

overall survival of tumor-bearing mice (Fig. 1E). To determine the impact of TBRI inhibition on the antitumor immune response, we harvested and analyzed the resected primary melanoma tissues for infiltrating effector $CD3^+CD8^+$ T-cell populations, as well as $CD4^+CD25^+FoxP3^+$ regulatory T cells (Treg) via multiparameter flow cytometry analysis. TBRI inhibition significantly increased the number of $CD8^+$ T cells in both primary melanoma and resected draining lymph nodes, with the $CD8^+$ T-cell/Treg ratio correlating closely with an inhibition of primary melanoma growth (Fig. 1F; Supplementary Fig. S1A). Similar findings were also obtained with the TBRI serine/threonine kinase inhibitor, LY2157299 monohydrate (Supplementary Fig. S1B–S1G). Overall, data suggest that TGFβ blockade enhances the antitumor immune response generated by anti–CTLA-4 immunotherapy.

TGFβ inhibition fails to augment anti–PD-1/PD-L1 blockade

Compared with CTLA-4 checkpoint blockade, anti–PD-1 and anti–PD-L1 therapies have generated improved objective responses and a superior side-effect profile in the clinic (27). However, our work showed modest response to anti–PD-1
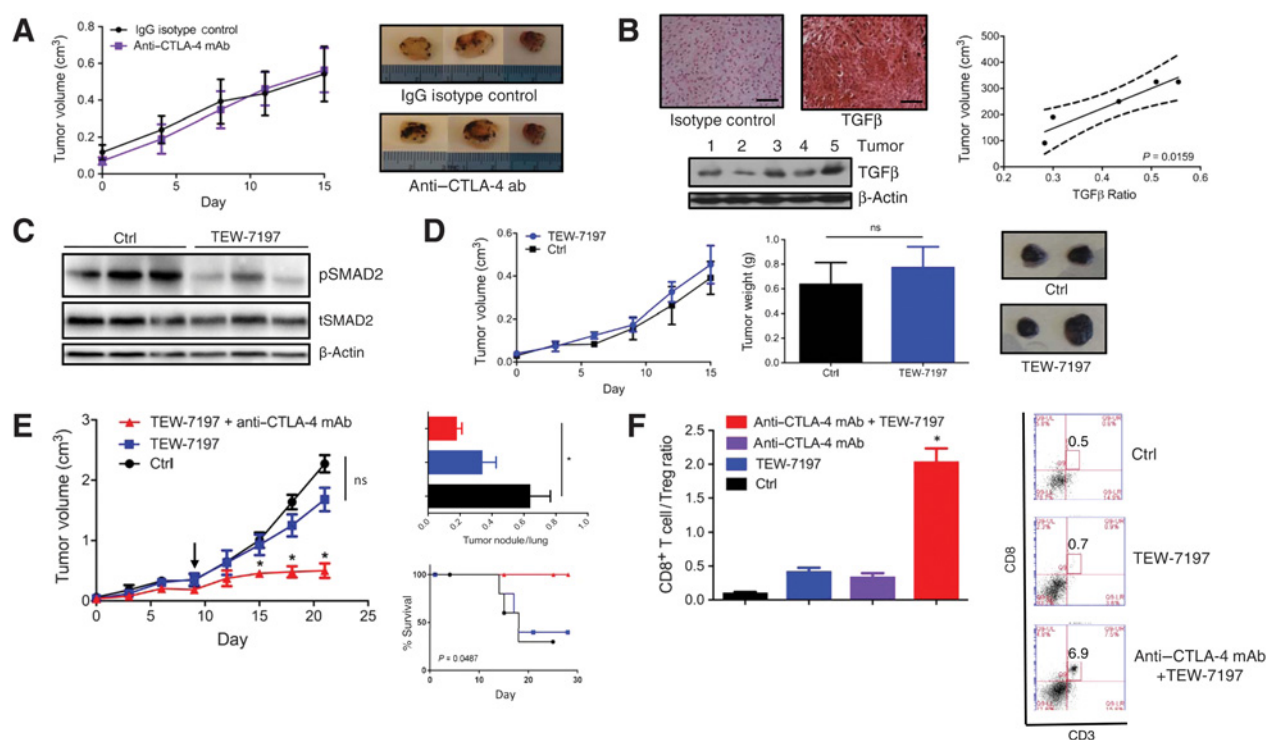

Figure 1.

TGFβ inhibition augments anti–CTLA-4 immunotherapy in an autochthonous BRAF^{V600E}PTEN$^{-/-}$ melanoma model. **A,** Mice were treated with either anti–CTLA-4 (purple, 100 μg i.p.) or IgG isotype control (black, 100 μg i.p.) every 3 days when tumors reached 60–80 mm^3. Left: tumor volumes monitored every 3 days. Right: representative tumor photos. Six mice/group. Representative of 3 independent experiments. **B,** Left: resected $Braf^{V600E}Pten^{-/-}$ melanoma tissues analyzed for TGFβ1 expression by IHC and whole tissue Western blots. IHC representative of 3 tumor specimens (40×). Right: Spearman correlation between tumor volume and TGFβ1/β-actin density ratios from Western blots. **C,** Phospho-SMAD2 (pSMAD2) Western blot analysis performed following TEW-7197 treatment (25 mg/kg daily p.o. × 2 weeks). tSMAD2: total SMAD2. Representative of 2 independent experiments. **D,** Left: mice were treated with TEW-7197 monotherapy (25 mg/kg daily p.o.). Tumor volumes were monitored every 3 days. Six mice/group. Representative of 3 independent experiments. Center: final tumor weights. Right: representative photos of resected tumors. ns: nonsignificant. **E,** Left: mice were treated with either IgG isotype control/vehicle control, TEW-7197(25 mg/kg p.o. daily) monotherapy, or combination anti–CTLA-4 (100 μg i.p. every 3 days)/TEW-7197. Left: tumor volumes monitored every 3 days. Six mice/group. Black arrow, treatment initiation. Representative of 2 independent experiments. Right top: lungs resected and enumerated for metastatic foci by staggered IHC. Right bottom: Kaplan–Meier survival plot. Data analyzed by the log-rank test. **F,** Left: flow cytometry on tumor-infiltrating lymphocytes (TILs) at the conclusion of the experiment. Five tumors/group. Right: representative flow diagrams. See Supplementary Fig. S1. All data are mean ± SEM. Significance calculated using the unpaired t test or a one-way ANOVA. *, $P < 0.05$.
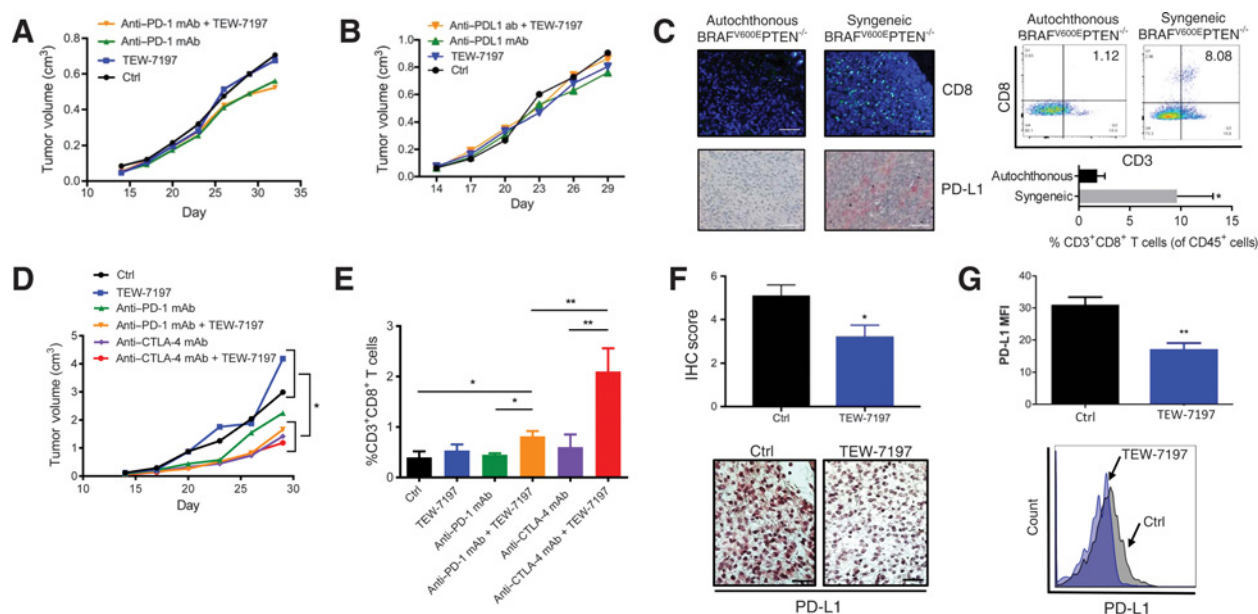
Figure 2.
TGFβ inhibition suppresses the PD-1/PD-L1 signaling axis and fails to augment anti–PD-1 immunotherapy in an autochthonous BRAF^{V600E}PTEN$^{-/-}$ melanoma model. **A,** Mice treated with either anti–PD-1(250 μg i.p.) or IgG isotype control (250 μg i.p.) every 3 days ± TEW-7197 (25 mg/kg p.o. daily) when tumors reach 60-80 mm^3. Tumor volumes monitored every 3 days. Six mice/group. Representative of 2 independent experiments. **B,** Mice treated with either anti–PD-L1 (200 μg i.p.) or IgG isotype control (200 μg i.p.) every 3 days ± TEW-7197(25 mg/kg p.o. daily). Tumor volumes monitored every 3 days. Six mice/group. Representative of 2 independent experiments. **C,** Left: autochthonous and syngeneic transplant $Braf^{V600E}Pten^{-/-}$ melanoma tissues were analyzed with CD8 immunofluorescence (10×) and PD-L1 IHC (20×). Representative of 3 tumors. Right top: flow cytometry of infiltrating CD45$^+$CD3$^+$CD8$^+$ T cells in both autochthonous and syngeneic $Braf^{V600E}Pten^{-/-}$ melanoma tissues. Gated on viable CD45$^+$ cells. Right bottom: CD3$^+$CD8$^+$ T cells (% of CD45$^+$ cells). **D,** Syngeneic $Braf^{V600E}Pten^{-/-}$ melanoma model treated with either anti–PD-1 (250 μg i.p.), anti–CTLA-4(100 μg i.p.), or IgG isotype control (250 μg i.p.) every 3 days ± TEW-7197 (25 mg/kg p.o. daily). Tumor volumes were monitored every 3 days. Seven mice/group. Representative of 2 independent experiments. **E,** Flow cytometry for TILs at the conclusion of the experiment in D. **F,** Mice from the autochthonous $Braf^{V600E}Pten^{-/-}$ melanoma model were treated with TEW-7197 (25 mg/kg p.o. daily × 2 weeks). Primary melanoma tissues were resected, scored (top), and analyzed for PD-L1 expression by IHC (red, bottom). Representative of 5 tumors (40×). IHC scores were calculated for 10 random fields in 5 tumors/group. **G,** Autochthonous $Braf^{V600E}Pten^{-/-}$ melanoma model was treated with TEW-7197 (25 mg/kg p.o. daily × 2 weeks). Primary melanoma tissues were resected and flow cytometry performed to quantitate PD-L1 surface expression on CD45$^-$EpCAM$^-$CD90.2$^-$ cells. Three tumors/group. Representative of 2 independent experiments. See Supplementary Fig. S2. All data are mean ± SEM. Significance calculated using an unpaired t test or a one-way ANOVA. *, $P < 0.05$; **, $P < 0.005$.

monotherapy in the autochthonous $Braf^{V600E}Pten^{-/-}$ melanoma model, and concurrent administration of the TEW-7197 TBRI inhibitor failed to significantly enhance the efficacy of PD-1/PD-L1 blockade (Fig. 2A and B). Based on previous studies, it was hypothesized that the lack of therapeutic benefit observed with anti–PD-1/PD-L1 in this autochthonous $Braf^{V600E}Pten^{-/-}$ melanoma model was associated with low numbers of tumor-infiltrating CD8$^+$ T cells and diminished PD-L1 surface expression. To confirm this hypothesis, we derived a $Braf^{V600E}Pten^{-/-}$ melanoma cell line from the corresponding autochthonous model, generated syngeneic $Braf^{V600E}PTEN^{-/-}$ melanomas, and found these tissues to harbor increased numbers of infiltrating CD8$^+$ T cells, along with enhanced PD-L1 expression relative to the autochthonous melanoma model (Fig. 2C). These findings correlated with the improved responses to anti–PD-1 monotherapy that were enhanced with the addition of TEW-7197 (Fig. 2D). Despite this more pronounced response to PD-1 blockade, the TEW-7197/anti–CTLA-4 combination generated a more robust antitumor immune response in this syngeneic $Braf^{V600E}Pten^{-/-}$ model (Fig. 2E). Because anti–CTLA-4 continued to provide superior responses when combined with TBRI inhibition relative to anti–PD-1 therapy, we conjectured that this phenomenon may

be related to alterations in tumor PD-L1 expression. We, therefore, conducted additional IHC and flow cytometry experiments and found that TEW-7197 treatment diminished the expression of surface PD-L1 expression in *in situ* melanoma tissues in the autochthonous $Braf^{V600E}Pten^{-/-}$ model (Fig. 2F and G). In line with reported findings, we also showed that the LY2157299 monohydrate inhibitor downregulated PD-1 expression on melanoma-infiltrating T cells (Supplementary Fig. S2; refs. 28, 29). These results suggest that the lack of synergy observed between TBRI inhibition and PD-1 blockade in this preclinical melanoma model is at least partially related to diminished PD-1/PD-L1 expression in the TME.

TGFβ inhibition expands local MAFs in an autochthonous melanoma model

While investigating the impact of TBRI inhibition on the generation of an antitumor immune response, we noted that TBRI inhibitor–treated melanoma tissues exhibited evidence of an expanded stromal compartment. This was initially demonstrated using trichrome staining and vimentin IHC, whereas evidence of MAF expansion was later seen using α-smooth muscle actin (α-SMA) and fibroblast-specific protein (FSP) IHC (Fig. 3A–C;
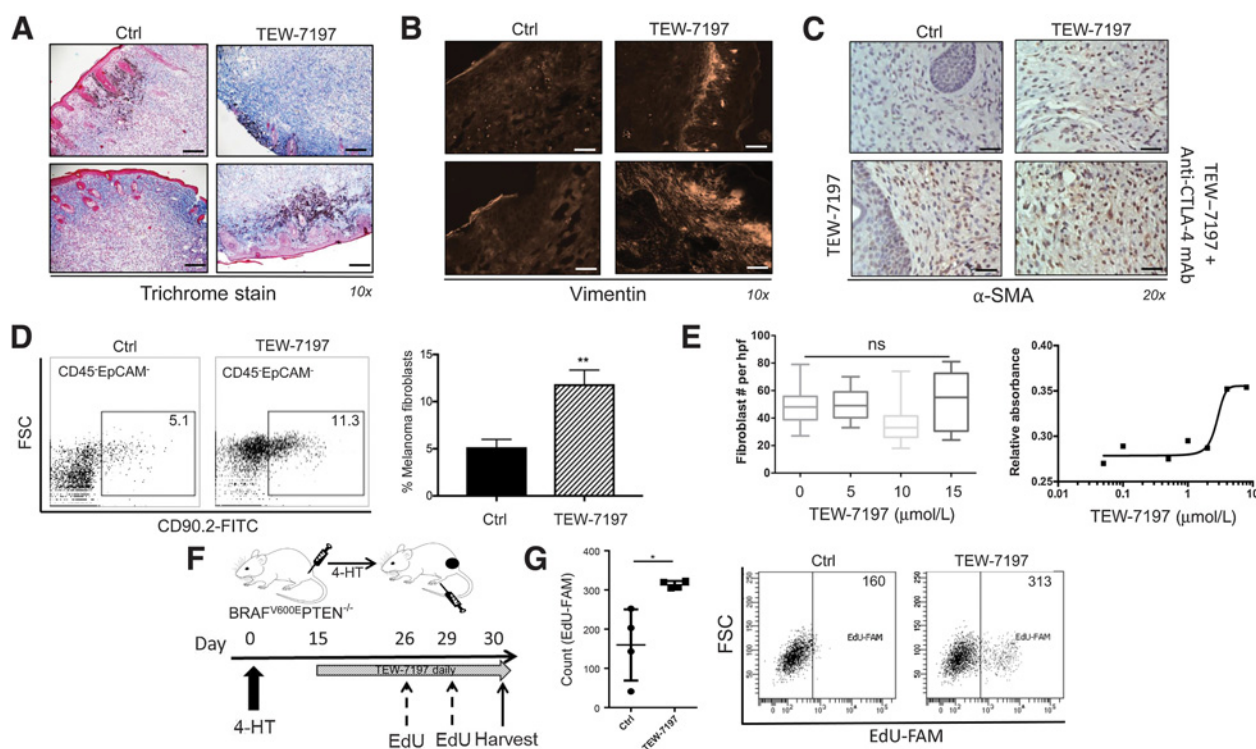
Figure 3.
TGFβ inhibition expands melanoma stromal fibroblasts. Autochthonous $Braf^{V600E}Pten^{-/-}$ melanoma model treated with TEW-7197 (25 mg/kg p.o. daily × 2 weeks), and tumors resected for (**A**) trichrome staining (blue: connective tissue), (**B**) vimentin IHC, and (**C**) α-SMA IHC. All histology are representative of 3 tumors/group and ≥6 sections/tumor. **D,** Autochthonous $Braf^{V600E}Pten^{-/-}$ melanoma model was treated with TEW-7197 (25 mg/kg p.o. daily × 2 weeks) versus a vehicle control, resected, and single-cell suspensions were generated. Flow cytometry used to quantitate $CD45^-EpCAM^-CD90.2^+$ MAFs. Three tumors/group. Representative of 2 independent experiments. **E,** Left: *in vitro* transwell migration assay. The $Braf^{V600E}Pten^{-/-}$ melanoma cell line treated with TEW-7197 and $Braf^{V600E}Pten^{-/-}$/MAF chemotaxis measured. Five wells/condition. Representative of 2 independent experiments. Right: *in vitro* proliferation assay. $Braf^{V600E}Pten^{-/-}$/MAFs treated with increasing concentrations of TEW-7197 and cellular proliferation was monitored by MTT assay. Three wells/condition. Representative of 3 independent experiments. **F,** Schematic of the *in vivo* MAF proliferation assay. 4-HT, 4-hydroxytamoxifen; EdU, 5-ethynyl-2′-deoxyuridine DNA incorporation dye. **G,** Quantitation of $EdU-FAM^+CD45^-EpCAM^-CD90.2^+$ proliferating MAFs in vehicle control and TEW-7197–treated autochthonous $Braf^{V600E}Pten^{-/-}$ melanomas. Four mice/group. Representative of 2 independent experiments. See Supplementary Figs. S3 and S4. All data are mean ± SEM. Significance calculated using an unpaired *t* test or a one-way ANOVA. *, $P < 0.05$; **, $P < 0.005$. ns: nonsignificant.

Supplementary Fig. S3). We also harvested TBRI inhibitor– and vehicle control–treated melanoma tissues from autochthonous $Braf^{V600E}Pten^{-/-}$ mice and performed multiparameter flow cytometry to quantitate the $CD45^-EpCAM^-CD90.2^+$ cells. Although the CD90.2 antigen has been detected on the surface of thymocytes, hematopoietic stem cells, and neurons, this surface antigen has also been used as a reliable fibroblast marker when excluding the $CD45^+$ cells (30). These studies supported our observation that TBRI inhibitor therapy enhanced the number of $CD45^-EpCAM^-CD90.2^+$ MAFs in the autochthonous $Braf^{V600E}Pten^{-/-}$ model (Fig. 3D). To further examine the impact of TBRI inhibitor therapy on MAFs, we expanded and isolated fibroblasts from resected autochthonous $Braf^{V600E}Pten^{-/-}$ melanoma tissues in culture. We subsequently enriched this population using microbeads selective to the CD90.2 surface antigen and confirmed elevated expression of α-SMA and vimentin (Supplementary Fig. S4A and S4B). This $Braf^{V600E}Pten^{-/-}$/MAF cell line was utilized in subsequent *in vitro* experiments demonstrating that TBRI inhibitor treatment promoted MAF proliferation, whereas no evidence of enhanced MAF recruitment was

detected in response to TBRI inhibitor treatment in transwell culture assays (Fig. 3E). Additional studies were conducted to measure the incorporation of the 5-ethynyl-2′-deoxyuridine (EdU) proliferation marker into $CD45^-EpCAM^-CD90.2^+$ MAFs within melanoma tissues resected from the autochthonous $Braf^{V600E}Pten^{-/-}$ model after treatment with TEW-7197 (Fig. 3F). These experiments confirmed that TBRI inhibition effectively enhanced MAF proliferation *in vivo* and indicated that TBRI inhibitors promoted the stromal expansion of this autochthonous $Braf^{V600E}Pten^{-/-}$ model by driving MAF proliferation. (Fig. 3G). Gene-expression studies to examine the effect of TGFβ inhibition on $Braf^{V600E}Pten^{-/-}$ tumors also revealed a compensatory increase in the expression of type II TGFβ receptor (*Tgfbr2*) expression, potentially contributing to enhanced MAF activation (Supplementary Fig. S4C). Altogether, these findings are consistent with the known role of autocrine TGFβ in regulating cellular homeostasis and are in line with a previous study reporting that genetic blockade of TGFβ signaling in mammary carcinoma-associated fibroblasts results in their *in vivo* expansion (31).
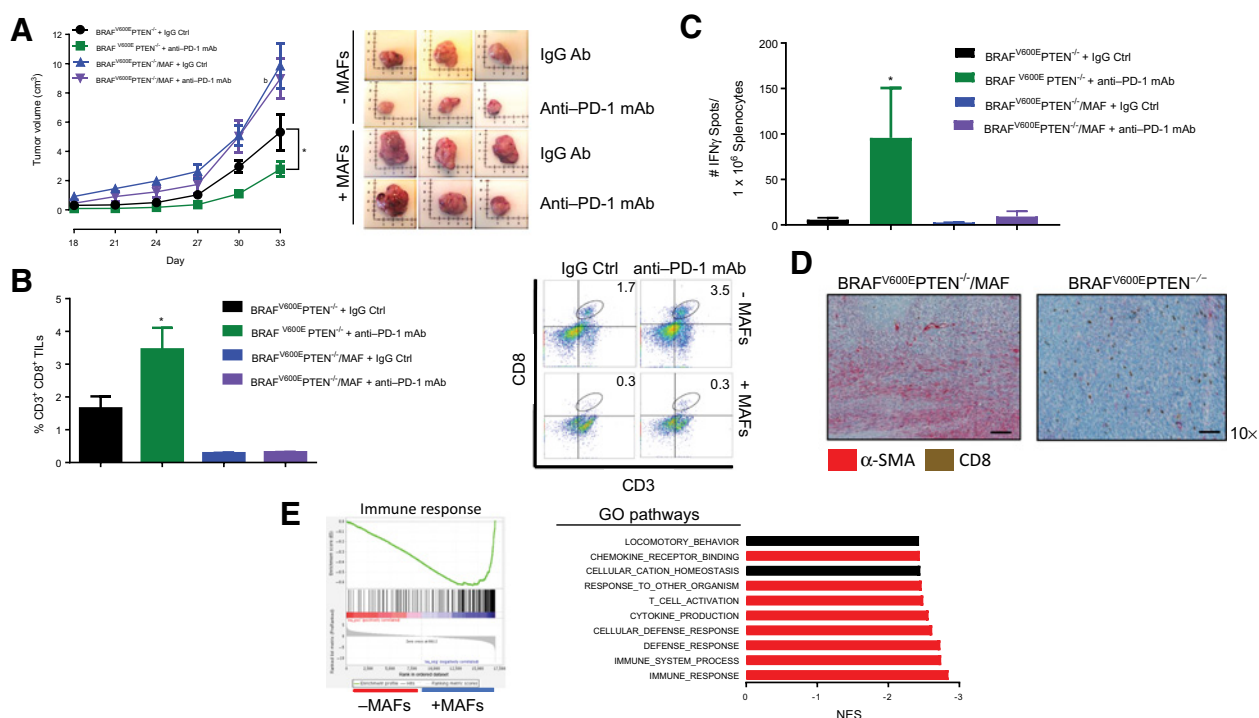
Figure 4.
MAFs suppress anti–PD-1 activity in the *Braf^V600E^Pten^−/−* melanoma model. **A,** *Braf^V600E^Pten^−/−* melanoma cells transplanted ± *Braf^V600E^Pten^−/−*/MAFs (1:3 ratio) into syngeneic C57BL/6 mice and treated with anti–PD-1 (250 μg i.p. every 3 days) or IgG isotype control (250 μg i.p. every 3 days) when tumors reach 60–80 mm³. Left: tumor volumes monitored every 3 days. Six mice/group. Representative of 2 independent experiments. Right, representative photos of resected primary melanomas. **B,** Flow cytometry for tumor-infiltrating CD3⁺CD8⁺ T cells from **A**. Right, representative flow diagrams. Five tumors/group. **C,** IFNγ by TRP2-specific T cells at the conclusion of the experiment in **A**. Splenocytes harvested from 5 mice/group. Representative of 2 independent experiments. **D,** Dual IHC analysis of α-SMA (red) and CD8 (brown) in *Braf^V600E^Pten^−/−*/MAF and *Braf^V600E^Pten^−/−* melanoma tissues. Three tumors/group. 10× images representative of 10 fields/tumor. **E,** RNA-seq analysis of *Braf^V600E^Pten^−/−*/MAF and *Braf^V600E^Pten^−/−* melanoma tissues. Left: enrichment plot showing downregulation of IMMUNE_RESPONSE GO pathway from *Braf^V600E^Pten^−/−*/MAF melanomas versus *Braf^V600E^Pten^−/−* melanomas. Right: association of the most downregulated GO pathways in cotransplanted BRAF^V600E^PTEN^−/−^/MAF melanomas with cellular immunity. NES: normalized enrichment score. All data are mean ± SEM. Significance calculated using a one-way ANOVA. *, $P < 0.05$.

MAFs suppress anti–PD-1 efficacy in a transgenic BRAF^V600E^PTEN^−/−^ melanoma model

Based on the lack of synergism observed between the TEW-7197 TBRI inhibitor and blockade of the PD-1/PD-L1 signaling axis, as well as the expansion of MAFs in response to TBRI inhibitor therapy, we hypothesized that MAFs may interfere with the efficacy of anti–PD-1/PD-L1 checkpoint inhibitor therapy. To test this hypothesis, we cotransplanted the previously generated *Braf^V600E^Pten^−/−*/MAF and *Braf^V600E^Pten^−/−* cell lines, as well as the *Braf^V600E^Pten^−/−* cell line alone, into syngeneic mice and examined the ability of these tumors to respond to anti–PD-1. MAFs significantly promoted primary tumor growth, while also diminishing the therapeutic efficacy of anti–PD-1 (Fig. 4A). MAF cotransplantation significantly reduced effector CD8⁺ T cells within primary melanomas and inhibited the observed induction of melanoma-infiltrating CD8⁺ T cells in response to anti–PD-1 (Fig. 4B). MAFs also diminished CD8⁺ T cells capable of recognizing the melanoma-associated antigen, tyrosinase-related protein-2 (TRP2; Fig. 4C), and impaired effector CD8⁺ T-cell infiltration within melanoma tissues (Fig. 4D). We conducted differential gene-expression analysis on *Braf^V600E^Pten^−/−* and *Braf^V600E^Pten^−/−*/MAF melanoma tissues using RNA-seq tran-

scriptomic sequencing. Gene pathway analysis revealed that 12 of the top 20 downregulated gene-expression pathways in the presence of MAFs were associated with the development of a cellular antitumor immune response (Fig. 4E). Taken together, these data suggest that MAFs significantly impair the generation of melanoma-specific T-cell responses and compromise the efficacy of anti–PD-1 checkpoint inhibition.

MAF MMP-9 suppresses PD-L1 expression and inhibits anti–PD-1 therapy

Clinical studies show a positive relationship between melanoma PD-L1 expression and responses to anti–PD-1 (32). Given that our findings have indicated that TBRI inhibition was associated with a concurrent increase in the number of MAFs, as well as diminished PD-L1 expression in the autochthonous *Braf^V600E^Pten^−/−* melanoma model (Figs. 2 and 3), we inquired whether MAFs could suppress local PD-L1 expression. Therefore, we performed coculture assays with the *Braf^V600E^Pten^−/−*/MAF and fluorophore-labeled *Braf^V600E^Pten^−/−* melanoma cell lines, followed by flow cytometry analysis of surface PD-L1 expression. Although no significant changes in fibroblast PD-L1 expression were noted, a consistent reduction
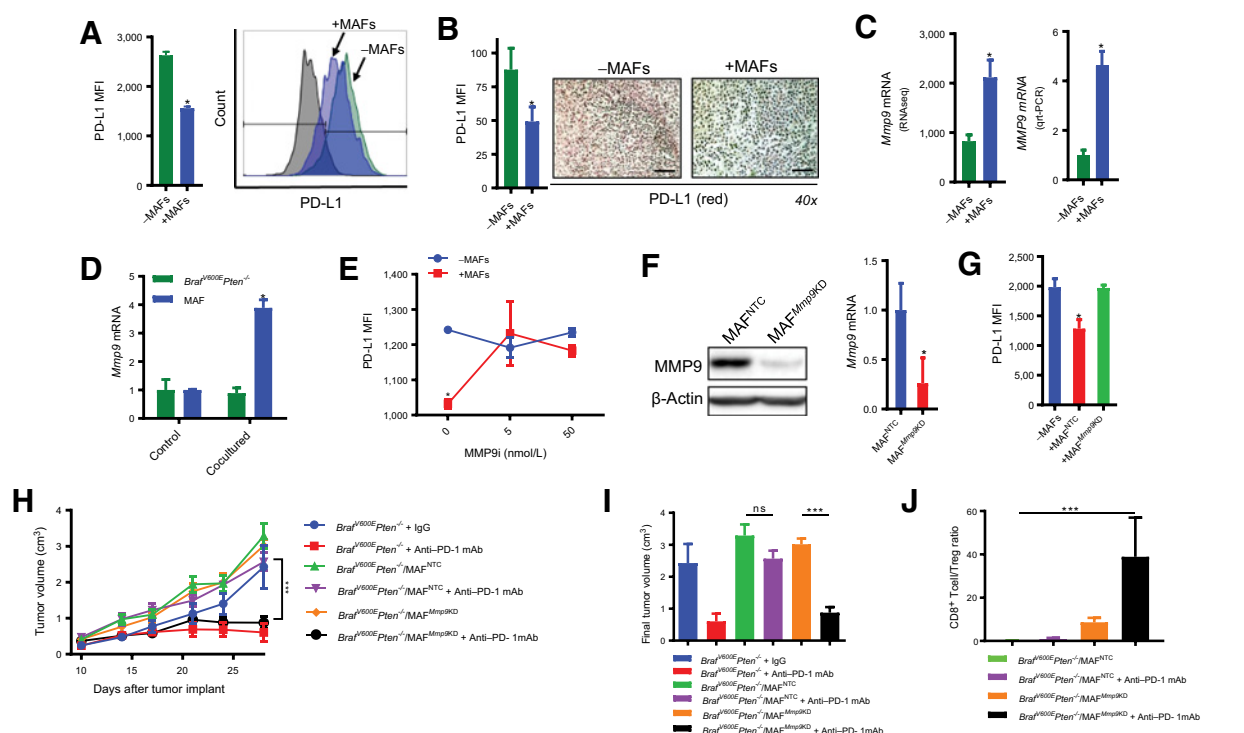
Zhao et al.

Figure 5.
Fibroblast MMP-9 negatively regulates melanoma surface PD-L1 expression. **A,** Left: PD-L1 expression from *in vitro* cocultures of $Braf^{V600E}Pten^{-/-}$ melanoma cells ± MAFs. Representative of 3 independent experiments. Right, flow diagram of $Braf^{V600E}Pten^{-/-}$ PD-L1 expression from different conditions. Black: unstained control; blue: +MAFs; green: −MAFs. **B,** Left: PD-L1 expression of *in vivo* $Braf^{V600E}Pten^{-/-}$ tumors ± MAFs. Five mice/group. Right, representative IHC of PD-L1 (40×). **C,** *Mmp9* mRNA expression of implanted $Braf^{V600E}Pten^{-/-}$ tumors ± MAFs from RNA-seq (left), validated by qRT-PCR (right). **D,** *Mmp9* mRNA expression by $Braf^{V600E}Pten^{-/-}$ tumor cells and MAFs when cultured separately or cocultured. Three independent replicates. **E,** PD-L1 expression of $BRAF^{V600E}PTEN^{-/-}±$MAFs with the indicated concentration of MMP9i (MMP9 inhibitor I). Three independent replicates. **F,** MMP-9 expression in stable cell lines $Braf^{V600E}Pten^{-/-}$-MAF^{NTC} (NTC: nontargeted control) and $Braf^{V600E}Pten^{-/-}$-MAF^{Mmp9KD} (KD, *Mmp9* knockdown). Left: Western blot. Right: qRT-PCR. **G,** PD-L1 expression by $Braf^{V600E}Pten^{-/-}$-melanoma cells following coculture with the $Braf^{V600E}Pten^{-/-}$-MAF^{NTC} and the $Braf^{V600E}Pten^{-/-}$-MAF^{Mmp9KD} cell lines. Representative of 3 independent experiments. **H,** Tumor measurements from $Braf^{V600E}Pten^{-/-}$ melanomas cotransplanted with either $Braf^{V600E}Pten^{-/-}$-MAF^{NTC} or $Braf^{V600E}Pten^{-/-}$-MAF^{Mmp9KD} fibroblasts treated with either IgG control or anti–PD-1. Five to 6 mice/group. **I,** Final tumor volumes from experiment in **H**. **J,** Flow cytometry for TILs performed at the conclusion of the experiment in **H**. See Supplementary Fig. S5. All data are mean ± SEM. Significance calculated using the unpaired *t* test or a one-way ANOVA. *, $P < 0.05$; ***, $P < 0.0005$.

in PD-L1 surface expression was found in $Braf^{V600E}Pten^{-/-}$ melanoma cells (Fig. 5A). A similar reduction in melanoma PD-L1 expression was also observed in $Braf^{V600E}Pten^{-/-}$ melanoma tissues cotransplanted with MAFs in syngeneic hosts (Fig. 5B). Further review of the RNA-seq differential gene expression in $Braf^{V600E}Pten^{-/-}$:$Braf^{V600E}Pten^{-/-}$/MAF cotransplanted tumors revealed a significant increase in the expression of matrix metalloproteinase-9 (MMP-9)/gelatinase B in cotransplanted $Braf^{V600E}Pten^{-/-}$/MAF melanoma tissues, a finding that was further confirmed by qRT-PCR (Fig. 5C). Based on these data, we performed $Braf^{V600E}Pten^{-/-}$: $Braf^{V600E}Pten^{-/-}$/MAF transwell coculture experiments and measured cell type–specific *Mmp9* expression by qRT-PCR analysis. $Braf^{V600E}Pten^{-/-}$/MAF cells expressed elevated *Mmp9* when exposed to $Braf^{V600E}Pten^{-/-}$ melanoma cells (Fig. 5D). Previous studies have noted a potential role of MMP enzymes in the regulation of surface PD-L1 expression (33). We, therefore, utilized a pharmacologic inhibitor to investigate the role of the MMP-9 enzyme in the downregulation of PD-L1 surface expression by $Braf^{V600E}Pten^{-/-}$ melanoma cells. Increasing concentrations of the MMP-9

inhibitor eliminated the suppressive effects of MAFs on melanoma cell PD-L1 surface expression (Fig. 5E), and genetic silencing of *Mmp9* expression in the $Braf^{V600E}Pten^{-/-}$/MAF cell line ($Braf^{V600E}Pten^{-/-}$/MAF^{MMP9KD} cells, Fig. 5F) abrogated the effect of MAFs on melanoma cell PD-L1 surface expression (Fig. 5G), supporting the hypothesis that MAF MMP-9 expression mitigated responses to anti–PD-1 therapy. Additional cotransplantation experiments showed that genetically silencing MAF *Mmp9* expression reversed the ability of MAFs to inhibit anti–PD-1 responses *in vivo* (Fig. 5H and I; Supplementary Fig. S5A). These effects on tumor development also correlated with an enhanced CD8$^+$ T-cell/Treg ratio in tumors comprised of MAFs with diminished *Mmp9* expression (Fig. 5J; Supplementary Fig. S5B). Although others have noted that MMP-13 may play a role in regulating PD-L1 surface expression, this enzyme had no impact on melanoma PD-L1 surface expression (Supplementary Fig. S5C; ref. 33). Altogether, these data suggest that MAF *Mmp9* expression plays an important role in determining responses to anti–PD-1 therapy.
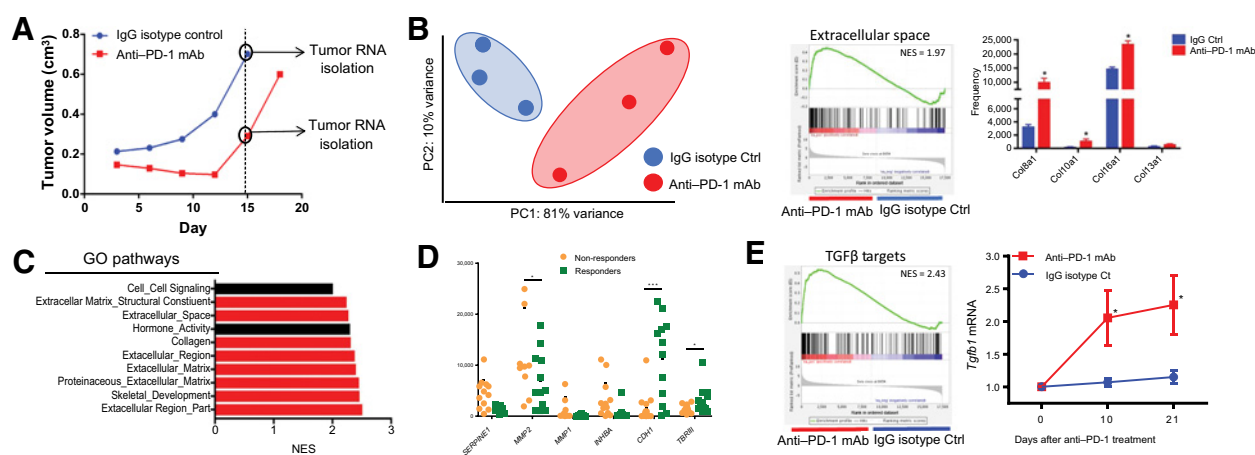
Cancer Immunology Research

Figure 6.
Stromal expansion and TGFβ signaling activation are associated with anti–PD-1 resistance. **A,** Autochthonous $Braf^{V600E}Pten^{-/-}$ melanoma model treated with either anti–PD-1(250 μg i.p. every 3 days) or IgG isotype control (250 μg i.p. every 3 days). Tumor volumes monitored every 3 days. Tumors resected following escape and progression during anti–PD-1 therapy, total RNA isolated, and RNA-seq analysis conducted. Three age/sex-matched mice/group. **B,** Left: principal component analysis of gene expression in response to anti–PD-1 versus IgG isotype control. Center: enrichment plot showing enhancement of Extracellular Space GO pathway upon anti–PD-1 treatment. Right: individual collagen-expressing genes in tumors treated with anti–PD-1 versus IgG isotype control. NES: normalized enrichment score. **C,** Upregulated gene expression in 13 anti–PD-1 refractory advanced melanoma patients based on GO term enrichment analysis of an available RNA-seq database (22). **D,** Genes associated with TGFβ signaling activation in anti–PD-1-treated melanoma patients in **C** (22). **E,** Left: enrichment plot showing enhancement of TGFβ gene-expression targets in the $Braf^{V600E}Pten^{-/-}$ melanoma model following escape from anti–PD-1 therapy. Right: serial biopsy $Tgfb1$ qRT-PCR analysis of the transgenic $Braf^{V600E}Pten^{-/-}$ melanomas undergoing treatment with the IgG isotype control or anti–PD-1. 6 mice/group. See Supplementary Fig. S6. All data are mean ± SEM. Significance calculated using the unpaired t test. *, $P < 0.05$; ***, $P < 0.0005$.

Stromal expansion and TGFβ activation are associated with resistance to anti–PD-1

Following a response to anti–PD-1 therapy, primary melanomas in the transgenic $Braf^{V600E}Pten^{-/-}$ model uniformly escaped and progressed (Fig. 6A). We harvested the $Braf^{V600E}Pten^{-/-}$ melanoma tissues following treatment with either anti–PD-1 or IgG isotype control antibody for subsequent RNA isolation and additional RNA-seq (Fig. 6A). Principal component analysis confirmed that anti–PD-1 induced significant alterations in gene expression in the autochthonous $Braf^{V600E}Pten^{-/-}$ melanoma model (Fig. 6B). This transcriptomic analysis further revealed that anti–PD-1–treated tumors exhibited a significant enrichment of a stromal gene-expression profile, including a statistically significant upregulation of several collagen-encoding genes and $S100a4$ (fibroblast-specific protein, FSP), as well as a trend toward significantly increased expression of Vim (vimentin) and $Acta2$ (α-SMA; Fig. 6B; Supplementary Fig. S6A–S6C). Further interrogation of a previously generated RNA-seq data set derived from the analysis of human melanoma tissues revealed $de\ novo$ resistance to anti–PD-1 to also be associated with the upregulation of several genes involved in the extracellular matrix, further supporting a relationship between the melanoma–stroma and the development of checkpoint inhibitor resistance (Fig. 6C; ref. 22). Given that TAFs within the tumor stroma have been shown to exhibit enhanced TGFβ expression (34), we investigated several genes regulated by or associated with the TGFβ signaling pathway and found these also correlated with primary resistance to anti–PD-1 (Fig. 6D). Based on these data, we further hypothesized that $Braf^{V600E}Pten^{-/-}$ melanomas that have escaped anti–PD-1 therapy will also exhibit enhanced TGFβ signaling activity. A transcriptomic gene-expression analysis of the anti–PD-1–treated autochthonous $Braf^{V600E}Pten^{-/-}$ melanoma model demonstrated

that anti–PD-1–refractory melanoma tissues also exhibited increased TGFβ signaling activity (Fig. 6E, left), and an assessment of serial biopsies of the same $Braf^{V600E}Pten^{-/-}$ melanoma model established that $Tgfb1$ expression was upregulated in a time-dependent manner upon escape from anti–PD-1 therapy (Fig. 6E, right).

Delayed inhibition of TGFβ signaling during anti–PD-1 therapy generates a more effective antitumor immune response

Taken together, these studies suggest that delayed TGFβ inhibitor therapy following checkpoint inhibitor treatment failure may generate a more effective overall antitumor response relative to upfront combination therapy. To address this question, we performed an additional experiment, where autochthonous $Braf^{V600E}Pten^{-/-}$ melanomas underwent anti–PD-1 therapy for 3 weeks followed by the daily administration of the TEW-7197 TBRI inhibitor. Whereas simultaneous combination anti–PD-1/TEW-7197 showed no evidence of response (Fig. 2A and B), delayed TEW-7197 administration in combination with continuous anti–PD-1 effectively controlled melanoma progression and suppressed primary tumor growth (Fig. 7A and B; Supplementary Fig. S7A). As opposed to the lack of an observed effect of continuous combination anti–PD-1/TEW-7197 therapy on antitumor T-cell responses, delayed TBRI inhibition, coinciding with anti–PD-1 resistance, resulted in a more robust expansion of melanoma-infiltrating effector CD8$^+$ T cells (Fig. 7C and D; Supplementary Fig. S7B). Delayed TEW-7197 treatment following escape from anti–PD-1 did not result in the stromal expansion of MAFs observed in concurrent anti–PD-1/TEW-7197 therapy or in tumors receiving TEW-7197 monotherapy (Fig. 7E–G; Supplementary Fig. S7C). This lack of MAF expansion also correlated with an
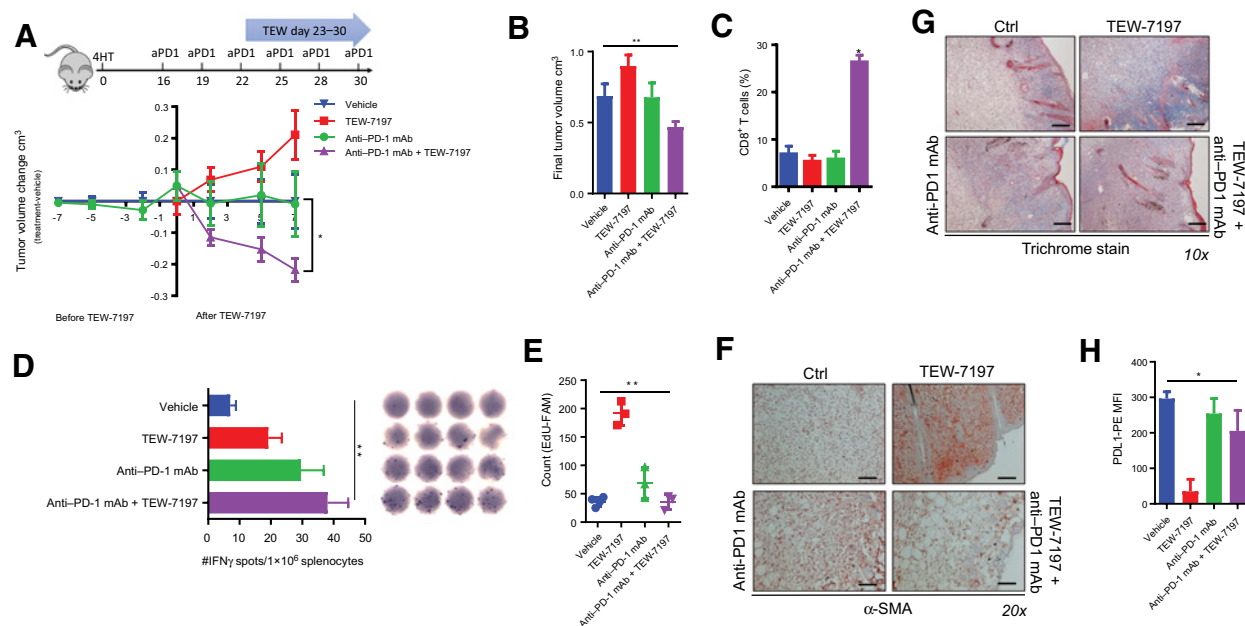
Figure 7.
Delayed dosing of the TGFβ inhibitor TEW-7197 improves anti–PD-1 therapy in the transgenic $Braf^{V600E}Pten^{-/-}$ melanoma model. **A,** Top: delayed dosing scheme of anti–PD-1 and TEW-7197. Bottom: tumor measurements before and after TEW-7197 initiation following previous anti–PD-1 therapy. Six mice/group. **B,** Final tumor volume measurements from **A**. **C,** Flow cytometry for TILs performed at the conclusion of the experiment in **A**. **D,** IFNγ ELISPOT analysis of TRP2-specific T cells performed in **A**. Splenocytes harvested from 5 mice/group. Representative of 2 independent experiments. **E,** Quantitation of EdU-FAM$^+$CD45$^-$EpCAM$^-$CD90.2$^+$ proliferating MAFs in autochthonous $Braf^{V600E}Pten^{-/-}$ melanomas following the indicated treatments as performed in **A**. Three tumors/group. Representative of 2 independent experiments. **F,** Tumor tissues resected for trichrome staining and **G,** α-SMA IHC. All histology representative of 3 tumors/group and at least 6 sections/tumor. **H,** Mice treated as indicated by the experiment described in **A**. Primary melanoma tissues resected at the same time points as in **A–D**. Flow cytometry utilized to quantitate PD-L1 surface expression on CD45$^-$EpCAM$^-$CD90.2$^-$ cells. Three tumors/group. See Supplementary Fig. S7. All data are mean ± SEM. Significance calculated using a one-way ANOVA. *, $P < 0.05$.

absence of *Mmp9* upregulation and a maintenance of melanoma cell PD-L1 surface expression in mice treated with the anti–PD-1/delayed TEW-7197 combination regimen (Fig. 7H; Supplementary Fig. S7D and S7E). These data further support the association between increased numbers of local MAFs and MMP-9–mediated downregulation of PD-L1 on the surface of tumor cells. Overall, these findings suggest that the sequencing of TGFβ inhibitors with checkpoint inhibitor immunotherapies may affect their overall effectiveness.

Discussion

Herein, we demonstrated that although TGFβ blockade effectively synergized with anti–CTLA-4 immunotherapy, it failed to augment anti–PD-1/PD-L1 immunotherapy in an autochthonous $Braf^{V600E}Pten^{-/-}$ melanoma model. Further mechanistic studies suggested that TGFβ inhibition drives the proliferative expansion of MAFs in this transgenic model and that this effect leads to diminished PD-L1 surface expression secondary to MMP-9–dependent cleavage. This potentially explains the observed lack of benefit derived from the TGFβ inhibitor–anti–PD-1/PD-L1 combination regimen. The elimination of MAF-mediated suppression of anti–PD-1 therapy following the genetic silencing of MAF *Mmp9* expression supports this claim. In line with previous studies, these data further showed that the development of anti–PD-1 resistance was associated with a genetic program that promotes mesenchymal transformation and is concomitant with enhanced TGFβ signaling activation. Delayed TGFβ inhibitor therapy, administered at the time of disease escape from anti–PD-1 therapy, more effectively controlled tumor development compared with continuous combination therapy in the same autochthonous $Braf^{V600E}Pten^{-/-}$ melanoma model. These data are consistent with reported findings supporting a role for stromal fibroblast TGFβ signaling and T-cell exclusion in certain solid tumors (35, 36).

Previous work has established that MMP-9 plays an important role in tumor angiogenesis and metastasis (37–39). However, the immune modulating effects of MMP-9 are less well understood (40, 41). The ability for MMP-9 to negatively regulate anti–PD-1 responses by diminishing the surface expression of tumor PD-L1 expression is consistent with the immunologic impact of other mechanisms elucidated to regulate the surface expression of this ligand (42–44). This effect of fibroblast MMP-9 on responses to anti–PD-1 suggests that a pharmacologic inhibitor of MMP-9 may combine favorably with checkpoint inhibitor therapy. An ongoing clinical trial is now investigating the combination of an antagonistic anti–MMP-9 (andecaliximab, GS-5745) with nivolumab in gastric and gastroesophageal junction adenocarcinoma (NCT02864381). This strategy seems particularly promising for the management of stroma-rich cancers, such as pancreatic cancer.

The present study is consistent with the data generated by Hugo and colleagues and implicates the process of mesenchymal transformation as supporting the development of checkpoint inhibitor resistance (22). The relationship between TGFβ signaling and the process of epithelial–mesenchymal transformation (EMT) is well established (45). This study also confirmed this relationship in the autochthonous $Braf^{V600E}Pten^{-/-}$ melanoma model, effectively associating escape of anti–PD-1 therapy with enhanced expression of mesenchymal markers, components of the extracellular stroma, and activation of the TGFβ signaling pathway. The translational relevance of this relationship was illustrated by showing that delayed TGFβ inhibitor therapy at the time of anti–PD-1 escape more effectively enhanced antitumor immune responses over those generated by continuous combination therapy. These findings have implications on clinical trial design, suggesting that TGFβ inhibitor therapies may offer more clinical benefit either in the second-line treatment setting or in those tumors preselected based on EMT-related markers. These data also suggest that a tissue biopsy at the time of disease progression will allow for improved selection of more effective immunotherapy regimens.

These findings should be considered in the context of the clinical data generated in patients with desmoplastic melanoma (DM), a subtype of melanoma characterized by its relationship with a spindled "fibroblastic" cytomorphology and an expanded collagenous extracellular matrix (46). Despite this dominant stromal phenotype, DMs have been associated with superior responses to anti–PD-1 checkpoint inhibition (47). We speculate that this relationship with enhanced efficacy of anti–PD-1 may be related to the increased mutational burden associated with this form of melanoma (48). This would be distinct from the low mutational burden in the transgenic melanoma model used in these studies and could explain the particularly potent inhibitory impact observed by MAFs. Nevertheless, investigators have been unable to identify a statistical difference in the mutational load between responding and nonresponding DM patients, suggesting that other factors contribute to modulating responses to checkpoint inhibitor therapy (47). It is likely that the interaction between several characteristics of the tumor, including but not limited to the mutational burden, PD-L1 surface expression, and the stromal compartment, all influence responses to checkpoint inhibitor therapies. It remains unclear why the MAFs in the $Braf^{V600E}Pten^{-/-}$ melanoma model are capable of suppressing the development of an effective CD8+ T-cell response, while the extensive stroma associated with DMs fail to impede this cytotoxic immune response. Differences in the biology between MAFs and the "fibroblastic" spindle cells within DMs are likely to contribute to these divergent responses to anti–PD-1. Previous electron microscopy studies have suggested that the stromal cells in DMs with fibroblastic features are dedifferentiated melanocytes rather than true fibroblasts (49–51).

Preclinical work has shown that TGFβ inhibition enhances antitumor immune responses generated by anti–PD-1/anti–PD-L1 therapies (52). We speculate that the lack of synergy observed in the current study, as opposed to previous reports, may be related to the use of a less immunogenic autochthonous tumor model that exhibited a stromal compartment that more closely recapitulated human disease. It can be inferred that the utilization of syngeneic transplant tumor models that harbor an increased number of infiltrating CD8+ T cells, while lacking any appreciable stromal compartment, is more likely to result in a more robust antitumor immune response relative to autochthonous tumor model systems. This is consistent with our observations that TEW-7197 augments the activity of anti–PD-1 in the transplant $Braf^{V600E}Pten^{-/-}$ melanoma model.

Prior work has established a role for TGFβ in promoting fibroblast activation and fibrosis. However, TGFβ also has an important role in negatively regulating cellular proliferation (53). In the autochthonous $Braf^{V600E}Pten^{-/-}$ melanoma model, we found that inhibiting TGFβ signaling had a more pronounced impact on MAF proliferation, an effect also described in the TAFs of a mammary carcinoma model engineered to be unresponsive to TGFβ signaling (31). It is possible that the increased stroma observed in melanomas exposed to TEW-7197 may be a result of both MAF proliferation and enhanced sensitivity to TGFβ ligands in response to downstream inhibition of TGFβ signaling. This would be supported by our finding that $Braf^{V600E}Pten^{-/-}$ melanomas treated with the TEW-7197 inhibitor exhibited enhanced Tgfbr2 expression. This would be consistent with elevated α-SMA expression observed in TEW-7197–treated melanomas. The resulting effect on stromal expansion would, therefore, represent a feedback effect elicited by potent pharmacologic inhibition of the TGFβ signaling pathway and may be more extensive after longer periods of treatment. Our analyses were performed at later time points, potentially explaining the observed stromal expansion in TEW-7197–treated melanomas.

It remains unknown whether the alterations in the tumor stroma as described in the current study are also observed in human tumor tissues in response to TGFβ inhibition, and it is unclear whether the differential efficacy observed between anti–CTLA-4 and anti–PD-1/PD-L1 therapies in combination with TGFβ inhibitors is also observed in cancer patients. Whether the effect on MAFs observed in this study is restricted to the small-molecule type I TGFβ serine/threonine kinase inhibitors or may also apply to the large-molecule TGFβ inhibitors is also undetermined. The current study is based on a single transgenic melanoma model that is likely to be more representative of melanomas with lower mutational burden. Further preclinical and clinical investigation is, therefore, necessary to understand the full potential of TGFβ inhibitor strategies in immuno-oncology. To this end, clinical trials are currently being conducted to examine the impact of concurrent TGFβ blockade on anti–PD-1 responses in patients with advanced malignancies. Although studies investigating the small-molecule type I TGFβ serine/threonine kinase inhibitors in combination with anti–PD-1 antibodies are still ongoing, early clinical data have been reported for M7824, a bifunctional fusion protein comprised of anti–PD-L1 and the extracellular domain of the type II TGFβ receptor that effectively functions as a TGFβ trap (52). Although clinical responses are being reported in pretreated patients with a variety of solid tumor types, larger studies with longer follow-up will be necessary to fully assess the clinical utility and ideal patient population of this therapeutic approach (54–57). This work underscores the importance of gaining a mechanistic understanding of the impact of pharmacologic agents on the tumor immune microenvironment and how these alterations may, in turn, affect the ultimate generation of effector antitumor immune responses. Developing this level of insight can greatly influence the development of the next generation of combination immunotherapy regimens.

Disclosure of Potential Conflicts of Interest

No potential conflicts of interest were disclosed.

Authors' Contributions

Conception and design: G.C. Blobe, B.A. Hanks

Development of methodology: F. Zhao, B.A. Hanks

Acquisition of data (provided animals, acquired and managed patients, provided facilities, etc.): F. Zhao, K. Evans, C. Xiao, N. DeVito, B. Theivanthiran, A. Holtzhausen, P.J. Siska, B.A. Hanks

Analysis and interpretation of data (e.g., statistical analysis, biostatistics, computational analysis): F. Zhao, N. DeVito, B. Theivanthiran, B.A. Hanks

Writing, review, and/or revision of the manuscript: F. Zhao, N. DeVito, G.C. Blobe, B.A. Hanks

Administrative, technical, or material support (i.e., reporting or organizing data, constructing databases): K. Evans, N. DeVito, B.A. Hanks

Study supervision: B.A. Hanks

References

1. Topalian SL, Sznol M, McDermott DF, Kluger HM, Carvajal RD, Sharfman WH, et al. Survival, durable tumor remission, and long-term safety in patients with advanced melanoma receiving nivolumab. J Clin Oncol 2014;32:1020–30.
2. Hodi FS, O'Day SJ, McDermott DF, Weber RW, Sosman JA, Haanen JB, et al. Improved survival with ipilimumab in patients with metastatic melanoma. N Engl J Med 2010;363:711–23.
3. Topalian SL, Hodi FS, Brahmer JR, Gettinger SN, Smith DC, McDermott DF, et al. Safety, activity, and immune correlates of anti-PD-1 antibody in cancer. N Engl J Med 2012;366:2443–54.
4. Syn NL, Teng MWL, Mok TSK, Soo RA. De-novo and acquired resistance to immune checkpoint targeting. Lancet Oncol 2017;18:e731–41.
5. Sharma P, Hu-Lieskovan S, Wargo JA, Ribas A. Primary, adaptive, and acquired resistance to cancer immunotherapy. Cell 2017;168:707–23.
6. Kyi C, Postow MA. Immune checkpoint inhibitor combinations in solid tumors: opportunities and challenges. Immunotherapy 2016;8: 821–37.
7. Ott PA, Hodi FS, Kaufman HL, Wigginton JM, Wolchok JD. Combination immunotherapy: a road map. J Immunother Cancer 2017;5:16.
8. Hanks BA, Holtzhausen A, Jamieson R, Gimpel P, Campbell O, Sun L, et al. Type III TGF-β receptor downregulation generates an immunotolerant tumor microenvironment. J Clin Invest 2013;123:3925–40.
9. Fontana A, Constam DB, Frei K, Malipiero U, Pfister HW. Modulation of the immune response by transforming growth factor beta. Int Arch Allergy Immunol 1992;99:1–7.
10. Kirkbride KC, Blobe GC. Inhibiting the TGF-beta signalling pathway as a means of cancer immunotherapy. Expert Opin Biol Ther 2003;3:251–61.
11. Flavell RA, Sanjabi S, Wrzesinski SH, Licona-Limon P. The polarization of immune cells in the tumour environment by TGFbeta. Nature Rev Immunol 2010;10:554–67.
12. Hanks BA, Morse MA. Pharmacological inhibition of TGFbeta as a strategy to augment the antitumor immune response. Curr Opin Investig Drugs 2010;11:1342–53.
13. Suarez C, Rodon J, Desjardins A, Forsyth P, Gueorguieva I, Cleverly A, et al. Phase 1b study evaluating safety and pharmacokinetics of the oral transforming growth factor-beta receptor I kinase inhibitor LY2157299 monohydrate when combined with chemoradiotherapy in newly diagnosed malignant gliomas. J Clin Oncol 2013;31:suppl; abstr 2039.
14. Herbertz S, Sawyer JS, Stauber AJ, Gueorguieva I, Driscoll KE, Estrem ST, et al. Clinical development of galunisertib (LY2157299 monohydrate), a small molecule inhibitor of transforming growth factor-beta signaling pathway. Drug Des Devel Ther 2015;9:4479–99.
15. Morris JC, Tan AR, Olencki TE, Shapiro GI, Dezube BJ, Reiss M, et al. Phase I study of GC1008 (fresolimumab): a human anti-transforming growth factor-beta (TGFbeta) monoclonal antibody in patients with advanced malignant melanoma or renal cell carcinoma. PLoS One 2014;9:e90353.
16. Turley SJ, Cremasco V, Astarita JL. Immunological hallmarks of stromal cells in the tumour microenvironment. Nat Rev Immunol 2015;15: 669–82.

17. Kraman M, Bambrough PJ, Arnold JN, Roberts EW, Magiera L, Jones JO, et al. Suppression of antitumor immunity by stromal cells expressing fibroblast activation protein-alpha. Science 2010;330:827–30.
18. Harper J, Sainson RC. Regulation of the anti-tumour immune response by cancer-associated fibroblasts. Semin Cancer Biol 2014;25:69–77.
19. Fearon DT. The carcinoma-associated fibroblast expressing fibroblast activation protein and escape from immune surveillance. Cancer Immunol Res 2014;2:187–93.
20. Feig C, Jones JO, Kraman M, Wells RJ, Deonarine A, Chan DS, et al. Targeting CXCL12 from FAP-expressing carcinoma-associated fibroblasts synergizes with anti-PD-L1 immunotherapy in pancreatic cancer. Proc Natl Acad Sci USA 2013;110:20212–7.
21. Tirosh I, Izar B, Prakadan SM, Wadsworth MH 2nd, Treacy D, Trombetta JJ, et al. Dissecting the multicellular ecosystem of metastatic melanoma by single-cell RNA-seq. Science 2016;352:189–96.
22. Hugo W, Zaretsky JM, Sun L, Song C, Moreno BH, Hu-Lieskovan S, et al. Genomic and transcriptomic features of response to anti-PD-1 therapy in metastatic melanoma. Cell 2016;165:35–44.
23. Holtzhausen A, Zhao F, Evans K, Tsutsui M, Orabona C, Tyler DS, et al. Melanoma-derived Wnt5a promotes local dendritic-cell expression of IDO and immunotolerance: opportunities for pharmacologic enhancement of immunotherapy. Cancer Immunol Res 2015;3:1082–95.
24. Allred DC, Harvey JM, Berardo M, Clark GM. Prognostic and predictive factors in breast cancer by immunohistochemical analysis. Mod Pathol 1998;11:155–68.
25. Mootha VK, Lindgren CM, Eriksson KF, Subramanian A, Sihag S, Lehar J, et al. PGC-1alpha-responsive genes involved in oxidative phosphorylation are coordinately downregulated in human diabetes. Nat Genet 2003;34:267–73.
26. Hanks BA, Holtzhausen A, Evans KS, Jamieson R, Gimpel P, Campbell OM, et al. Type III TGF-beta receptor downregulation generates an immunotolerant tumor microenvironment. J Clin Invest 2013;123:3925–40.
27. Weber JS, Kahler KC, Hauschild A. Management of immune-related adverse events and kinetics of response with ipilimumab. J Clin Oncol 2012;30:2691–7.
28. Park BV, Freeman ZT, Ghasemzadeh A, Chattergoon MA, Rutebemberwa A, Steigner J, et al. TGFbeta1-Mediated SMAD3 Enhances PD-1 expression on antigen-specific T cells in cancer. Cancer Discov 2016;6:1366–81.
29. Stephen TL, Payne KK, Chaurio RA, Allegrezza MJ, Zhu H, Perez-Sanz J, et al. SATB1 expression governs epigenetic repression of PD-1 in tumor-reactive T cells. Immunity 2017;46:51–64.
30. Kisselbach L, Merges M, Bossie A, Boyd A. CD90 Expression on human primary cells and elimination of contaminating fibroblasts from cell cultures. Cytotechnology 2009;59:31–44.
31. Cheng N, Bhowmick NA, Chytil A, Gorksa AE, Brown KA, Muraoka R, et al. Loss of TGF-beta type II receptor in fibroblasts promotes mammary carcinoma growth and invasion through upregulation of TGF-alpha-, MSP-and HGF-mediated signaling networks. Oncogene 2005;24:5053–68.
32. Teng MW, Ngiow SF, Ribas A, Smyth MJ. Classifying cancers based on T-cell infiltration and PD-L1. Cancer Res 2015;75:2139–45.

33. Dezutter-Dambuyant C, Durand I, Alberti L, Bendriss-Vermare N, Valladeau-Guilemond J, Duc A, et al. A novel regulation of PD-1 ligands on mesenchymal stromal cells through MMP-mediated proteolytic cleavage. Oncoimmunology 2016;5:e1091146.

34. Bierie B, Moses HL. Tumour microenvironment: TGFbeta: the molecular Jekyll and Hyde of cancer. Nat Rev Cancer 2006;6:506–20.

35. Mariathasan S, Turley SJ, Nickles D, Castiglioni A, Yuen K, Wang Y, et al. TGFbeta attenuates tumour response to PD-L1 blockade by contributing to exclusion of T cells. Nature 2018;554:544–8.

36. Tauriello DVF, Palomo-Ponce S, Stork D, Berenguer-Llergo A, Badia-Ramentol J, Iglesias M, et al. TGFbeta drives immune evasion in genetically reconstituted colon cancer metastasis. Nature 2018;554:538–43.

37. Hiratsuka S, Nakamura K, Iwai S, Murakami M, Itoh T, Kijima H, et al. MMP9 induction by vascular endothelial growth factor receptor-1 is involved in lung-specific metastasis. Cancer Cell 2002;2:289–300.

38. Bergers G, Brekken R, McMahon G, Vu TH, Itoh T, Tamaki K, et al. Matrix metalloproteinase-9 triggers the angiogenic switch during carcinogenesis. Nat Cell Biol 2000;2:737–44.

39. Safina A, Ren MQ, Vandette E, Bakin AV. TAK1 is required for TGF-beta 1-mediated regulation of matrix metalloproteinase-9 and metastasis. Oncogene 2008;27:1198–207.

40. Creighton C, Hanash S. Expression of matrix metalloproteinase 9 (MMP-9/gelatinase B) in adenocarcinomas strongly correlated with expression of immune response genes. In Silico Biol 2003;3:301–11.

41. Sun D, Wang X, Zhang H, Deng L, Zhang Y. MMP9 mediates MICA shedding in human osteosarcomas. Cell Biol Int 2011;35:569–74.

42. Casey SC, Tong L, Li Y, Do R, Walz S, Fitzgerald KN, et al. MYC regulates the antitumor immune response through CD47 and PD-L1. Science 2016;352:227–31.

43. Dorand RD, Nthale J, Myers JT, Barkauskas DS, Avril S, Chirieleison SM, et al. Cdk5 disruption attenuates tumor PD-L1 expression and promotes antitumor immunity. Science 2016;353:399–403.

44. Li CW, Lim SO, Xia W, Lee HH, Chan LC, Kuo CW, et al. Glycosylation and stabilization of programmed death ligand-1 suppresses T-cell activity. Nat Commun 2016;7:12632.

45. Zavadil J, Bottinger EP. TGF-beta and epithelial-to-mesenchymal transitions. Oncogene 2005;24:5764–74.

46. Frydenlund N, Leone D, Yang S, Hoang MP, Deng A, Hernandez-Perez M, et al. Tumoral PD-L1 expression in desmoplastic melanoma is associated with depth of invasion, tumor-infiltrating CD8 cytotoxic lymphocytes and the mixed cytomorphological variant. Mod Pathol 2017;30:357–69.

47. Eroglu Z, Zaretsky JM, Hu-Lieskovan S, Kim DW, Algazi A, Johnson DB, et al. High response rate to PD-1 blockade in desmoplastic melanomas. Nature 2018;553:347–50.

48. Shain AH, Garrido M, Botton T, Talevich E, Yeh I, Sanborn JZ, et al. Exome sequencing of desmoplastic melanoma identifies recurrent NFKBIE promoter mutations and diverse activating mutations in the MAPK pathway. Nat Genet 2015;47:1194–9.

49. Valensi QJ. Desmoplastic malignant melanoma: A light and electron microscopic study of two cases. Cancer 1979;43:1148–55.

50. Bryant E, Ronan SG, Felix EL, Manaligod JR. Desmoplastic malignant melanoma: a study by conventional and electron microscopy. Am J Dermatopathol 1982;4:467–74.

51. Busam KJ, Mujumdar U, Hummer AJ, Nobrega J, Hawkins WG, Coit DG, et al. Cutaneous desmoplastic melanoma: reappraisal of morphologic heterogeneity and prognostic factors. Am J Surg Pathol 2004;28:1518–25.

52. Lan Y, Zhang D, Xu C, Hance KW, Marelli B, Qi J, et al. Enhanced preclinical antitumor activity of M7824, a bifunctional fusion protein simultaneously targeting PD-L1 and TGF-beta. Sci Transl Med 2018;10:eaan5488.

53. Medicherla S, Li L, Ma JY, Kapoun AM, Gaspar NJ, Liu YW, et al. Antitumor activity of TGF-beta inhibitor is dependent on the microenvironment. Anticancer Res 2007;27:4149–57.

54. Strauss J, Heery CR, Schlom J, Madan RA, Cao L, Kang Z, et al. Phase I trial of M7824 (MSB0011359C), a bifunctional fusion protein targeting PD-L1 and TGFbeta, in advanced solid tumors. Clin Cancer Res 2018;24:1287–95.

55. Gulley JL, Heery CR, Schlom J, Madan RA, Cao L, Lamping E, et al. Preliminary results from a phase I trial of M7824 (MSB0011359C), a bifunctional fusion protein targeting PD-L1 and TGF-beta in advanced solid tumors. J Clin Oncol 2017;35 suppl: 3006.

56. Fujiwara Y, Koyama T, Helwig C, Watanabe M, Doi T. M7824 (MSB0011359C), a bifunctional fusion protein targeting PD-L1 and TGF-β, in Asian patients with advanced solid tumors. J Clin Oncol 2018;36 suppl:762.

57. Kopetz S, Spira A, Wertheim M, Kim ES, Tan B, Heinz-Josef L, et al. M7824 (MSB0011359C), a bifunctional fusion protein targeting PD-L1 and TGF-β, in patients with heavily pretreated CRC: Preliminary results from a phase I trial. J Clin Oncol 2018;36 suppl:764.